Resistive drift-wave turbulence

Suzana J. Camargo, Dieter Biskamp, and Bruce D. Scott
Max-Planck-Institut für Plasmaphysik 85748 Garching bei München, Germany

(Received 20 June 1994; accepted 26 September 1994)

Two-dimensional resistive drift-wave turbulence is studied by high-resolution numerical simulations in the limit of small viscosity. Density and potential fluctuations are cross-coupled by resistive dissipation, proportional to the adiabaticity parameter, $\mathscr{C}$, which determines the character of the system: adiabatic ($\mathscr{C}\gg 1$) or hydrodynamic ($\mathscr{C}\ll 1$). Various cases are computed for $0.1\leqslant\mathscr{C}\leqslant 5$. Energy spectra exhibit a maximum at some wave number $k_0(\mathscr{C})$ and an inertial range behavior for $k>k_0$. The transfer of energy and vorticity is directly computed and confirms the persistence of local cascade dynamics in all regimes: the familiar dual cascade for the **E×B** flow eddies, and the direct cascade to small scales for the density as it is advected by the eddies. Inertial range spectral power laws agree surprisingly well with simple scaling predictions. No prominent large-scale long-lived coherent structures are observed, an absence that is consistent with the statistical properties, which are found to be perfectly Gaussian for $k\lesssim k_0$, but exhibit the non-Gaussian behavior, typical for small-scale intermittency, in the inertial range. © *1995 American Institute of Physics.*

I. INTRODUCTION

The energy losses observed in magnetically confinement devices, such as tokamaks and stellerators, are much greater than predicted by neoclassical transport theory and usually attributed to the presence of small-scale plasma turbulence (see, e.g., Ref. 1). It is also well known that spatial gradients in the plasma lead to collective modes called drift waves, which have wave numbers in the range of the observed density fluctuations. Therefore, drift-wave turbulence is considered as a natural cause of anomalous transport, in particular, in the cool plasma edge region.[2,3]

A particularly simple model has been proposed by Hasegawa and Wakatani,[4,5] describing two-dimensional (2-D) drift-wave turbulence in a collision dominated plasma with an unsheared magnetic field. This is an autonomous system describing excitation and damping of modes in terms of a few collisionality parameters, leading to a stationary turbulence level without external driving. In this paper, the Hasegawa–Wakatani equations are studied by high-resolution numerical simulations in the limit of small viscosity, i.e., high Reynolds numbers, which we call the nonviscous limit. Here the only relevant parameter is the adiabaticity parameter $\mathscr{C}$. For $\mathscr{C}\gg 1$, the adiabatic regime, the Hasegawa–Wakatani system, reduces to the Hasegawa–Mima system,[6] while for $\mathscr{C}\ll 1$, the hydrodynamic regime, it reduces essentially to a 2-D Navier–Stokes equation for the **E×B** flow eddies and a passive advection equation for the density fluctuations.

The Hasegawa–Wakatani model has recently been studied using numerical simulations, both as a diagnostic tool for the more complex situation involving magnetic shear,[7] and, in its own right as a model for tokamak edge turbulence.[8] In the former study, an earlier analysis of statistical equilibrium ensembles,[9] arguing cascade tendencies of the two nonlinear operators, was confirmed via direct simulation without dissipation for $\mathscr{C}=0$ and $\mathscr{C}=\infty$, which stressed their competing and opposite tendencies, and the fact that these tendencies persist in both extremes (see below). The main feature discovered and discussed by the second study was the emergence and persistence of long-lived large-scale coherent structures, which occur, in particular, in the hydrodynamic regime and appear to reduce the turbulent transport substantially. In those simulations, the turbulence properties were, however, strongly determined by plasma viscosity and density diffusivity, in addition to the adiabaticity parameter. By contrast, one of the results of this paper is that no such structures exist when these dissipative effects are reduced.

In addition, we find that the saturation level of the total energy is minimum for $\mathscr{C}\sim 1$ and increases in both the hydrodynamic and the adiabatic limits. By contrast, the saturation levels of the enstrophy and the turbulent flux are maximum in the hydrodynamic limit, and diminishes as $\mathscr{C}$ increases. The energy and the enstrophy spectra exhibit maxima at some intermediate wave number k_0 and a power law decay toward both small and large k. On the high-k side, the spectral properties closely follow simple scaling predictions. The turbulent density flux agrees well with the quasilinear estimate at the large scales for all $\mathscr{C}$. At the small scales, however, the quasilinear estimate exceeds the turbulent flux by a constant factor that increases with decreasing $\mathscr{C}$, while there is agreement over the entire spectrum in the adiabatic limit. The statistics of potential, density and vorticity increments over distances l are purely Gaussian for large scales ($l\gtrsim k_0^{-1}$), while they are increasingly non-Gaussian for small scales ($l<k_0^{-1}$), confirming the usual picture of intermittency.

We also directly compute the transfer of kinetic and density fluctuation energy and of **E×B** fluid vorticity between different length scales in the saturated turbulent state for each computed case. The results show clearly that the transfer always occurs as a local cascade between length scales within a factor of 2 of each other, and that the basic character of each nonlinearity remains the same in all regimes, with only the relative strength sensitive to $\mathscr{C}$. This extends the previous result for dissipationless systems[7] to the more real-

 1070-664X/95/2(1)/48/15/$6.00

istic situation in which all the effects of the Hasegawa–Wakatani system are present. The system behaves as a forced turbulent bath always with the same properties, while only the degree of statistical independence between potential and density fluctuations is affected by the presence of dissipative cross-coupling.

In Sec. II the Hasegawa–Wakatani model is described. The linear analysis of this system is presented in Sec. III. The simulation details are discussed in Sec. IV. Section V is devoted to the basic properties of the saturated turbulent state and how it varies with $\mathscr{C}$. Comparison of the results to quasilinear predictions is covered in Sec. VI, and the statistical properties are described in Sec. VII. Spectral transfer phenomena are treated in Sec. VIII. Finally, the conclusions are in Sec. IX. Some of the results presented here already appeared in Ref. 10.

II. HASEGAWA–WAKATANI SYSTEM

The model of our numerical studies of resistive drift-wave turbulence is the Hasegawa–Wakatani system in slab geometry.[4,5] The equilibrium magnetic field, $\mathbf{B}=B\hat{\mathbf{z}}$, is constant in the z direction, and magnetic fluctuations are neglected. The equilibrium density n_0 is nonuniform with a density gradient dn_0/dx in the negative x direction, such that the equilibrium density scale $L_n=n_0/|dn_0/dx|$ is constant. The simplifications of cold ions and isothermal electrons are taken, so that finite Larmor radius effects and temperature gradients and fluctuations are neglected: $T_i \ll T_e \equiv T$. The time evolution is then described by two coupled nonlinear equations for the fluctuations of the potential $\tilde{\phi}(x,y)$ and the density $\tilde{n}(x,y)$:[4,5]

$$\frac{\partial}{\partial t}\nabla_\perp^2\tilde{\phi}+(\hat{\mathbf{z}}\times\nabla_\perp\tilde{\phi})\cdot\nabla_\perp\nabla_\perp^2\tilde{\phi}=\mathscr{C}(\tilde{\phi}-\tilde{n})+\mathscr{D}^{\phi}, \tag{1}$$

$$\frac{\partial}{\partial t}\tilde{n}+(\hat{\mathbf{z}}\times\nabla_\perp\tilde{\phi})\cdot\nabla_\perp\tilde{n}+\frac{\partial\tilde{\phi}}{\partial y}=\mathscr{C}(\tilde{\phi}-\tilde{n})+\mathscr{D}^{n}, \tag{2}$$

where the usual dimensionless variables are defined as

$$x\to\frac{x}{\rho_s},\quad y\to\frac{y}{\rho_s},\quad t\to t\,\frac{c_s}{L_n}, \tag{3}$$

and the normalized potential and density fluctuations are given by

$$\tilde{\phi}=\frac{e\phi}{T}\frac{L_n}{\rho_s},\quad \tilde{n}=\frac{n}{n_0}\frac{L_n}{\rho_s}. \tag{4}$$

Here, the drift-wave dispersion scale ρ_s and sound speed c_s are given by $\rho_s^2=c^2M_iT/e^2B^2$ and $c_s^2=T/M_i$, respectively.

Equations (1) and (2) are linearly cross-coupled through the adiabaticity parameter,

$$\mathscr{C}=\frac{T}{n_0e^2\eta_\parallel}\frac{k_\parallel^2}{c_s/L_n}, \tag{5}$$

and the fluctuation length scales are assumed to satisfy the usual drift ordering, $k_\parallel \ll k_\perp$.

Equation (2) is the electron continuity equation, whose right side represents the effect of parallel electron compressibility $\nabla_\parallel v_{e\parallel}$, determined by force balance on the electrons (the Ohm's law):

$$\eta_\parallel\tilde{J}_\parallel\equiv-ne\tilde{v}_\parallel=\tilde{E}_\parallel+\frac{1}{ne}\nabla_\parallel\tilde{p}=\frac{T}{ne}\nabla_\parallel\tilde{n}-\nabla_\parallel\tilde{\phi}, \tag{6}$$

Eq. (1) is the quasineutrality condition, in which perpendicular divergence of the ion polarization drift balances parallel compression in the electrons. The polarization drift v_p results from an expansion of the ion equation of motion in ρ_s/L_n, yielding $v_p/v_E=\mathscr{O}(\rho_s/L_n)$, where v_E is the $\mathbf{E}\times\mathbf{B}$ drift. Both v_p and v_E contribute to the same order in the continuity equation because of the incompressibility of v_E, therefore the disparity in scale is compensated by that in size. It is important to note that in the cold-ion limit Eq. (1) is valid for arbitrary $k\rho_s$.

In the weakly collisional limit $\mathscr{C}\gg 1$, the electron response is nearly adiabatic ($\tilde{n}\to\tilde{\phi}$), and Eqs. (1) and (2) reduce to the Hasegawa–Mima equation.[6] In the strongly collisional limit $\mathscr{C}\ll 1$, Eq. (1) reduces to the 2-D Navier–Stokes equation for the $\mathbf{E}\times\mathbf{B}$ flow, by which $\tilde{n}$ is passively advected.

There are four different invariants of the system, and these can be combined in two relevant invariants with evolution equations which can be easily interpreted in terms of source and sink terms. The invariants of the purely nonlinear subset of the Hasegawa–Wakatani system are then the total energy,

$$E=\frac{1}{2}\int d^2x(\tilde{n}^2+|\nabla_\perp\tilde{\phi}|^2), \tag{7}$$

and the generalized enstrophy,

$$U=\frac{1}{2}\int d^2x(\tilde{n}-\nabla_\perp^2\tilde{\phi})^2\equiv\frac{1}{2}\int d^2x(\tilde{n}-\tilde{\Omega})^2, \tag{8}$$

with $\tilde{\Omega}$ the $\mathbf{E}\times\mathbf{B}$ vorticity (these are explicit invariants of the pure Hasegawa–Mima system). Under Eqs. (1) and (2), these quantities evolve with time as

$$\frac{\partial E}{\partial t}=\Gamma_n-\Gamma_c-\mathscr{D}^E, \tag{9}$$

$$\frac{\partial U}{\partial t}=\Gamma_n-\mathscr{D}^U, \tag{10}$$

where

$$\Gamma_n=-\int d^2x\;\tilde{n}\left(\frac{\partial\tilde{\phi}}{\partial y}\right), \tag{11}$$

$$\Gamma_c=\mathscr{C}\int d^2x(\tilde{n}-\tilde{\phi})^2, \tag{12}$$

$$\mathscr{D}^E=\int d^2x(\tilde{n}\mathscr{D}^n-\tilde{\phi}\mathscr{D}^{\phi})=\mathscr{D}_N^E+\mathscr{D}_V^E, \tag{13}$$

$$\mathscr{D}^U=-\int d^2x(\tilde{n}-\tilde{\Omega})(\mathscr{D}^n-\mathscr{D}^{\phi}). \tag{14}$$

These four quantities constitute the sources and sinks with which the turbulence interacts.[7] Only Γ_n can act as a source; the other quantities are sinks. The first, Γ_n, is the rate at which fluctuation energy extracts free energy available in the gradient (it is proportional to the gradient, which is unity in normalized units). The second, Γ_c, is the rate at which fluctuation energy is resistively dissipated. These first two quantities represent the collisional drift wave energetics in the nonviscous limit. It is important to note that they are active, only to the extent that the dynamics is nonadiabatic: if $\tilde{n}=\tilde{\phi}$, then both Γ_n and Γ_c vanish, leaving one with the Hasegawa–Mima system, up to viscous dissipation. In this spirit, fine dynamics studies are aided by the use of the nonadiabatic part of the density fluctuation, $\tilde{h}$, defined as

$$\tilde{h}=\tilde{n}-\tilde{\phi}, \tag{15}$$

after which one can substitute $\tilde{h}$ for $\tilde{n}$ in the definition for Γ_n and for $\tilde{n}-\tilde{\phi}$ in that for Γ_c. One should also note that the nonlinear advection of $\tilde{n}$ by the $\mathbf{E}\times\mathbf{B}$ flow vanishes identically for adiabatic electrons; this will be important to the interpretation of the results, especially concerning energy transfer phenomena. Concerning Γ_n and Γ_c, one minor difference exists from previous work: since we are interested in comparisons to the quasilinear flux, we do not express the Γ's as amplitude growth rates, as was done previously in order to compare with linear growth rates.[7,11]

The other two sinks, $\mathscr{D}^E$ and $\mathscr{D}^U$, collectively constitute "viscous" dissipation: they are contributed to by $\mathscr{D}^n$ and $\mathscr{D}^\phi$. Physically, these arise through collisional diffusion of electrons perpendicular to $\mathbf{B}$ and ion viscosity, respectively.[12] For typical tokamak edge parameters, both of these are very small,[11] to the point that their retention would necessitate much finer grids than are necessary: The nonviscous limit, in which $\mathscr{D}^E$ and $\mathscr{D}^U$ are negligible compared to Γ_n and Γ_c, requires only that the spectrum be truncated at some $k_{\max}>\rho_s^{-1}$. How this is done is unimportant. For this reason, we introduce the following high-order diffusion operators:

$$\mathscr{D}^\phi=\nu_\phi\,\nabla_\perp^6\tilde{\Omega}, \quad \mathscr{D}^n=\nu_n\,\nabla_\perp^6\tilde{n}, \tag{16}$$

and we choose

$$\nu_\phi=\nu_n=\nu, \tag{17}$$

such that by taking appropriate values of ν, dissipation can be confined to the smallest scales resolved in the numerical system. We can thus arrange that for sufficiently high spatial resolution, the energy dissipation $\mathscr{D}^E$ in Eq. (9) becomes negligible. On the other hand, one can see from Eq. (10) that $\mathscr{D}^U$ must remain finite: It has been shown by statistical studies[9] and confirmed by numerical simulation[7] that, in the absence of dissipation, the enstrophy spectrum is $U_k\sim k$, basically different from the decreasing spectrum $U_k\sim k^{-\mu}$, with $\mu\sim 3$ observed for weakly dissipative systems. In this paper, the interest is focused on conditions, such that $\mathscr{D}^E\simeq 0$, $\mathscr{D}^U$ finite, which we call the nonviscous limit. Here the only salient parameter is $\mathscr{C}$; ν determines only the extent of the inertial range of the energy and the enstrophy spectra.

III. LINEAR ANALYSIS

It is interesting to solve the linearized system analytically, in order to see the modal distribution of sources and sinks of the system's linear waves and the linear density response function. This is useful in comparison to the mode structure of the turbulence, as well as between the nonlinear turbulent flux and the correspondent quasilinear expressions, which are often used in simplified transport models.[1–3]

A. Dispersion relation

Linearization and Fourier decomposition of Eqs. (1) and (2), assuming a modal dependence of the type $e^{i(\mathbf{k}\cdot\mathbf{x}-\omega t)}$, leads to a dispersion relation, which has two solutions corresponding to unstable and strongly damped modes. The unstable modes are the only remaining after the system develops for a finite time. They are characterized by a real frequency ω_r and a growth rate γ:

$$\omega_+=\omega_r+i\gamma, \tag{18}$$

where

$$\omega_r=\mathscr{A}\sqrt{\mathscr{B}-1}, \tag{19}$$

$$\gamma=-\lambda/2+\mathscr{A}\sqrt{\mathscr{B}+1}, \tag{20}$$

in which

$$\mathscr{A}=\lambda_0/2\sqrt{2}, \tag{21}$$

$$\mathscr{B}=\sqrt{1+\frac{16\sigma^2}{\lambda_0^4}}, \tag{22}$$

$$\lambda=\lambda_0+\lambda_1=\frac{\mathscr{C}(1+k_\perp^2)}{k_\perp^2}+2\nu k_\perp^6, \tag{23}$$

$$\sigma=\mathscr{C}k_y/k_\perp^2. \tag{24}$$

The linear results are presented in Fig. 1. The behavior of γ for $k_x=0$ for $\nu=0$ is shown as a function of $\mathscr{C}$ in Fig. 1(a). In Fig. 1(b), the maximum linear growth rate is shown as a function of the adiabaticity parameter $\mathscr{C}$ and in Fig. 1(c), the values of wave number $\mathbf{k}_m=(0,k_m)$ of the maximum growth rate as a function of $\mathscr{C}$. The dependence of the linear growth rate on the dissipation coefficient ν is shown in Fig. 1(d).

B. Linear density response

From the linear analysis, it is possible to obtain an expression for the relation between $\tilde{n}_\mathbf{k}$ and $\tilde{\phi}_\mathbf{k}$: the linear density response expressed as $\tilde{n}_\mathbf{k}(\tilde{\phi}_\mathbf{k})$. Similarly, the nonadiabatic response may be expressed as $\tilde{h}_\mathbf{k}(\tilde{\phi}_\mathbf{k})$. These are compared to the corresponding relations for the turbulence in subsequent sections.

The nonadiabatic linear density response function [defined in (15)], is given by

$$\tilde{h}_\mathbf{k}=\frac{ik_y-(i\omega-\nu k_\perp^6)(1+k_\perp^2)}{i\omega-\nu k_\perp^6}\,\tilde{\phi}_\mathbf{k}. \tag{25}$$

The total linear density response is then expressed as

$$\tilde{n}_\mathbf{k}=(1+f_\mathbf{k})\tilde{\phi}_\mathbf{k}, \tag{26}$$

where

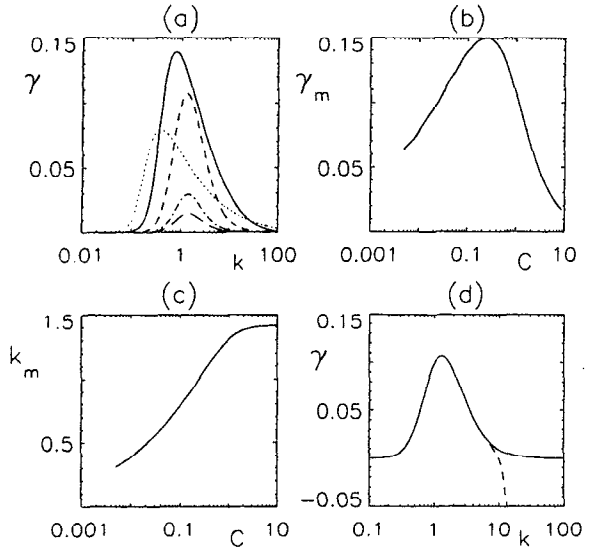

FIG. 1. (a) Linear growth rate γ for $k_x=0$, different values of $\mathscr{C}$ and $\nu=0$, $\mathscr{C}=0.01$ (dots), $\mathscr{C}=0.1$ (full line), $\mathscr{C}=1$ (short dashes), $\mathscr{C}=5$ (short/long dashes), and $\mathscr{C}=10$ (long dashes). (b) Maximum linear growth rate γ_m for $k_x=0$ as a function of $\mathscr{C}$, for $\nu=0$. (c) k_m, k_y of the maximum growth rate as a function of $\mathscr{C}$, for $\nu=0$. (d) Linear growth rate γ, for $k_x=0$, $\mathscr{C}=1$, $\nu=0$ (full line), and $\nu=1E-8$ (dashed line).

$$f_{\mathbf{k}}=-(1+k_\perp^2)+\frac{\omega_r k_y}{(\gamma+\nu k_\perp^6)^2+\omega_r^2}-i\,\frac{(\gamma+\nu k_\perp^6)k_y}{(\gamma+\nu k_\perp^6)^2+\omega_r^2}, \tag{27}$$

where for each $\mathbf{k}$, γ, and ω_r are those in Eqs. (20) and (19), respectively.

C. Phase shifts

In most transport modeling, it is assumed that the nonadiabatic response is small, entering purely as a shift in phase between $\tilde{n}_{\mathbf{k}}$ and $\tilde{\phi}_{\mathbf{k}}$:

$$\tilde{n}_{\mathbf{k}}=(1-i\delta)\tilde{\phi}_{\mathbf{k}}, \quad \delta\ll 1, \tag{28}$$

with a given δ for each Fourier component.[13] In this paradigm, drift waves are thought of as principally ion dynamics described by the Hasegawa–Mima system with electrons entering only in terms of the small phase shift, such that the linear waves or turbulence can tap free energy in the gradients. However, the energetics represented by Eqs. (11) and (12) indicate that drift-wave dynamics are based on the electrons, and the ions enter only through the inertia, in order to keep the system quasineutral.

In general, $\tilde{n}_{\mathbf{k}}$ and $\tilde{\phi}_{\mathbf{k}}$ are two complex numbers whose ratio can be given in terms of an amplitude and a phase shift, and the phase shift may be expressed as

$$\delta_{\mathbf{k}}=\mathrm{Im}\,\log \tilde{n}_{\mathbf{k}}^*\tilde{\phi}_{\mathbf{k}}, \tag{29}$$

and directly evaluated from the computations. In the turbulence it is clearly a function of time, so statistical averages are taken.

For linear waves, the superscript "L" is used to distinguish from the turbulence, and the phase shift $\delta_{\mathbf{k}}^L$ is obtained from the response function $f_{\mathbf{k}}$:

$$\delta_{\mathbf{k}}^L=-\mathrm{Im}\,\log(1+f_{\mathbf{k}}). \tag{30}$$

This linear phase shift also holds in the case of a quasilinear model, in which $\tilde{\phi}$ is turbulent, but $\tilde{n}(\tilde{\phi})$ is assumed to be linear.

With these definitions, it will be possible to check the validity of the i-delta model, since it will be clear whether the amplitude ratio between $\tilde{n}_{\mathbf{k}}$ and $\tilde{\phi}_{\mathbf{k}}$ is close to unity and whether $\delta_{\mathbf{k}}$ is small. It is already known that the i-delta model is a disastrous failure for the case of a sheared magnetic field.[14]

IV. SIMULATION DETAILS

Equations (1) and (2) were solved on a square box of size $L^2=(2\pi/K_0)^2$ with periodic boundary conditions, using a dealiased pseudospectral algorithm, similar to the one employed for a sheared magnetic field.[15] The grid size (number of collocation points, or nodes) varied from 128^2 (coarse-grid) to 1024^2 (fine-grid) nodes. Two different box sizes were used to concentrate primarily either on high-k (small-box) and low-k (large-box) properties; with $K_0=0.15$ and 0.0375, respectively. The dissipation parameter ν was kept just large enough to prevent numerical instability at the scale of the node spacing. This varied between $\nu=5\times10^{-10}$ for fine-grid, small-box runs, to $\nu=10^{-4}$ for coarse-grid, large-box runs. In order to reproduce the results of Koniges *et al.*[8] additional runs were taken with $K_0=0.1$, and different dissipation operators of the form $\mathscr{D}^\phi=\nu\nabla_\perp^4(\nabla_\perp^2\tilde{\phi})$ and $\mathscr{D}^n=\nu\,\nabla_\perp^2\tilde{n}$, with $\nu\sim0.1$.

Three values of $\mathscr{C}$ were used in the computations, representing the hydrodynamic ($\mathscr{C}=0.1$) and adiabatic ($\mathscr{C}=5$) regimes, with an additional case in the transition regime ($\mathscr{C}=1$). In the adiabatic regime, the slow system response limited the value of $\mathscr{C}$ to 5, since obtaining good statistics in the saturated state, would otherwise be too expensive. This slowness of response can be understood from the linear growth rates, which decrease rapidly with $\mathscr{C}$, as well as by the fact that in the near-adiabatic limit, spectral transfer in the density fluctuations is suppressed by the dissipative cross-coupling (nonlinear $\mathbf{E}\times\mathbf{B}$ advection of $\tilde{n}$ vanishes as $\tilde{n}\to\tilde{\phi}$). In the hydrodynamic regime, $\mathscr{C}$ was limited to 0.1 for a different reason: to keep the system in the nonviscous limit $\mathscr{D}^E$ must be small compared to Γ_c in the energy equation, Eq. (9). An additional case with high resolution and $\mathscr{C}=0.01$ was considered for comparison with Ref. 8. Though in this case, $\mathscr{D}^E$ is not negligible compared to the other terms in the energy equation, coherent structures were not observed, and the main characteristics are the same described in the case $\mathscr{C}=0.1$.

The numerical simulations were initialized with a random-phase, broadband field for the density and the potential fluctuations. The initial state was adiabatic and isotropic, exciting all degrees of freedom with a constant amplitude, such that

$$\sum_{\mathbf{k}}\tilde{\phi}_{\mathbf{k}}\tilde{\phi}_{\mathbf{k}}^*=\frac{1}{2}, \tag{31}$$

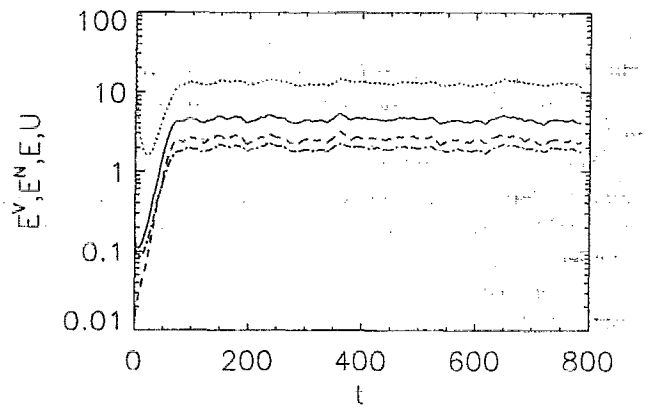

FIG. 2. Time evolution of the total energy E (full line), the kinetic energy E^V (short/long dashes), the density energy E^N (long dashes), and the enstrophy U (dots) is shown for $\mathscr{C}=1$; $\nu=10^{-8}$, $K_0=0.15$, and 512^2 grid points.

and $\tilde{n}_{\mathbf{k}}=\tilde{\phi}_{\mathbf{k}}$. A typical numerical simulation was started with 128^2 grid points and dissipation coefficient $\nu\sim10^{-4}$. After the linear phase, a saturated turbulent state is reached and maintained for a long enough time to obtain good statistical averages for the fluctuating quantities ($t\sim1500$). The number of nodes was then increased to 256^2 and ν reduced to $\nu\sim10^{-6}$. A new saturated state was reached in a short time ($t\sim80$ for $\mathscr{C}=5$ and $t\sim20$ for $\mathscr{C}=1$), with an energy level not appreciably different from that established prior to the changes. Further changes took the system to 512^2 nodes and $\nu\sim10^{-8}$, and finally to 1024^2 nodes and $\nu\sim10^{-10}$. Some of the diagnostics, such as the energy and enstrophy spectra, respond almost immediately to the changes, and need only short computation time to be accurate. Global quantities, such as the total energy, which depend mainly on low-k (large-scale) modes require longer times to give accurate average values. Hence, the 1024^2-node cases are presented mainly to investigate small-scale properties such as inertial range spectra and high-k statistics, which respond quickly to system changes. Test runs with 512^2 grid points were also performed from the initial conditions to confirm that the extended mode number space does not alter the saturation process. The numerical error was tracked in all runs by using the energy equation, Eq. (9). The mismatch (due to the artificial dissipation and numerical error) was never greater than $0.02E$.

V. THE SATURATED STATE

In this section we describe the basic properties of the saturated turbulent state: amplitude and energy levels, and spectra of both the energy components and the source and sink rates. The results discussed in this section are obtained from cases with 512^2 nodes for $\nu=10^{-8}$ and $K_0=0.15$, with only $\mathscr{C}$ varying. We refer often to the cascade dynamics of the system; although these are not covered in detail until Sec. VIII, they are already known in broad measure.[9,7]

Because of the low initial amplitude and the broad presence of unstable modes, the evolution of the system follows a standard pattern: a linear growth phase followed by nonlinear saturation. In Fig. 2, the typical time evolution of the energies and the enstrophy is illustrated for the transitional case, $\mathscr{C}=1$. Due to the initial excitation of the high-k modes, the enstrophy, U, is quite large but then decays rapidly due to the finite ν, and the efficiency of the vorticity cascade to small scales.

TABLE I. Saturation and fluctuation values for $K_0=0.15$, $\nu=10^{-8}$, and 512^2 grid points in the three different regimes.

$\mathscr{C}$	0.1	1	5
E	23.8	4.4	8.3
δE	20%	16%	8%
E^N	20.0	2.5	6.4
E^N/E	0.84	0.57	0.77
E^V	3.8	1.9	1.9
E^V/E	0.16	0.43	0.23
U	42.0	12.8	12.7
δU	18%	13%	8%
Γ_n	2.9	0.73	0.13
$\delta\Gamma_n$	43%	25%	35%
Γ_c	2.2	0.72	0.13
$\delta\Gamma_c$	26%	21%	40%
$\mathscr{D}^E$	0.6	0.0055	0.000 35
$\mathscr{D}^E/\Gamma_n$	21%	0.7%	0.3%
$\mathscr{D}_N^E/\mathscr{D}^E$	99.7%	76.4%	0.6%
$\mathscr{D}_V^E/\mathscr{D}^E$	0.3%	23.6%	99.4%
$\mathscr{D}^U$	2.8	0.72	0.13
Γ^{ql}	7.2	1.0	0.13

Saturated levels of the global quantities such as E, U, and the Γ's are given in Table I. In addition to these levels, the speed with which the system enters saturation is strongly dependent on $\mathscr{C}$. The saturation time strongly decreases with $\mathscr{C}$, primarily for the reason that the ability of $\tilde{n}$ to decouple from $\tilde{\phi}$, and hence to cascade to small scales is much greater in the hydrodynamic regime. This is not explained by the linear growth rates, since γ peaks for intermediate $\mathscr{C}$ and then drops away to either side. This is a first indication that the system's evolution is decided by its nonlinear properties. A second indication is that for the three cases considered the saturated energy level, E, is minimum for $\mathscr{C}=1$, in opposite tendency to the strength of γ. One notes that the variation in E with $\mathscr{C}$ is almost entirely due to that in E^N, and that temporal fluctuation of E is greatest in the hydrodynamic regime; this indicates that the dissipative cross-coupling is of primary importance. When $\tilde{n}$ is allowed, statistical independence from $\tilde{\phi}$ the system is at its most robust. The saturated enstrophy, on the other hand, decreases uniformly toward the adiabatic limit. This is due to the presence of the vorticity cascade to small scales in all regimes, coupled with the lower Γ_n in the adiabatic regime. Both Γ_n and Γ_c decrease toward the adiabatic limit, as they depend on a finite $\tilde{h}$, but Γ_c also depends on a finite $\mathscr{C}$, so it is strongest for $\mathscr{C}=1$.

Comparison of the levels of viscous dissipation (Table I), D_N^E and D_N^E, to the Γ's and to E indicates the role of spectral transfer: D_N^E, and hence D^E, is lowest in the adiabatic regime due to the weak cascade power in $\tilde{n}$, which is strongly coupled to $\tilde{\phi}$ with its 2-D fluid inverse energy cascade. So although the source rate Γ_n is weak in the adiabatic regime, the dominant energy transfer is toward large scales and Γ_c is also weak, so that the energy level E is comparatively large. This situation of high-energy level and weak energy transfer is responsible for the slow system response in the adiabatic

regime. While in the hydrodynamic regime, D^E is mostly due to D_N^E, in the adiabatic regime D_V^E is strongest, since the loss of the direct cascade in $\tilde{n}$ has removed D_N^E. As one would expect from the always-robust vorticity cascade, the enstrophy dissipation is not negligible in any regime.

The transitional case $\mathscr{C}=1$ has the strongest combination of dissipation—Γ_c and cascade to small scales, hence exciting D^E—and weakened driving, Γ_n, and so its saturated energy level is the lowest. All this serves to demonstrate that nonlinear drive and damping rates, not linear growth rates, together with the strength of interscale spectral transfer, are what determine the character of the saturated state.

As originally pointed out by Hasegawa and Wakatani,[5] the spatial structure of $\tilde{\phi}$ and $\tilde{n}$ is clear from the contour plots, which are shown in Figs. 3 and 4. The structure of $\tilde{\phi}$ and $\tilde{\Omega}$ are not strongly dependent on the regime; $\tilde{\phi}$ collects at large scales and $\tilde{\Omega}$ collects at small scales, reflecting the 2-D $\mathbf{E}\times\mathbf{B}$ fluid's dual cascade. The contours of $\tilde{n}$, however, show the results of the strength or weakness of the cross-coupling; in the hydrodynamic regime, $\tilde{n}$ exhibits pronounced gradient sheets, the characteristic feature of a passively advected scalar as it is cascaded to small scales. In the adiabatic regime the cross-coupling forces $\tilde{n}$ to mimic $\tilde{\phi}$.

All of these considerations are also apparent from the energy and enstrophy spectra, which are shown in Fig. 5. We define an angle-integrated spectrum for each of these quantities; for example, the spectrum of E^N is given by summing the contributions from each mode $\mathbf{k}$ whose magnitude falls within Δk of k:

$$E^N=\int dk\, E_k^N \rightarrow \sum_k E_k^N, \tag{32}$$

$$E_k^N=\int_{\mathbf{k}} d^2k\, E_{\mathbf{k}}^N \rightarrow \sum_{\mathbf{k}} E_{\mathbf{k}}^N, \quad k-\Delta k<|\mathbf{k}|<k+\Delta k, \tag{33}$$

$$E_{\mathbf{k}}^N=\tfrac{1}{2}|\tilde{n}_{\mathbf{k}}|^2, \tag{34}$$

and similarly for E^V with

$$E_{\mathbf{k}}^V=\tfrac{1}{2}|\mathbf{k}\tilde{\phi}_{\mathbf{k}}|^2. \tag{35}$$

Similar expressions are defined for the other E's, U, and the Γ's and D's, and in these expressions $\Delta k=0.5K_0$.

Generally, E_k exhibits a maximum at a certain wave number $k=k_0$. On the high-k side of this, there is an inertial range in which E_k follows a decaying power law ($E_k\sim k^{-\alpha}$) up to the viscous cutoff, k_ν, introduced by the increasing strength of D^E with k. The variation of the spectral exponent α with $\mathscr{C}$ is compiled in Table II.

To understand the dependence of E_k on $\mathscr{C}$, we consider E_k^V and E_k^N separately. The power exponent for E_k^V is not very sensitive, varying only between $\alpha_V=3.1$ and 3.5. This is due to the fact that for all three cases, the cascade dynamics for $\tilde{\phi}$ are similar, and the source/sink rates are negligible in the inertial range (which is, of course, a matter of definition; this is quantified in Sec. VIII). Indeed, that there is an inertial range, even for $\mathscr{C}>1$, results from the smallness of Γ_c, where the efficient cross-coupling keeps $\tilde{h}$ small: again, in the limit $\mathscr{C}\rightarrow\infty$, Eqs. (1) and (2) simply reduce to the Hasegawa–Mima equation, and in the opposite limit, Eq. (1) reduces to the 2-D Navier–Stokes equation. For the 2-D Navier–Stokes system, a simple self-similar vorticity cas-

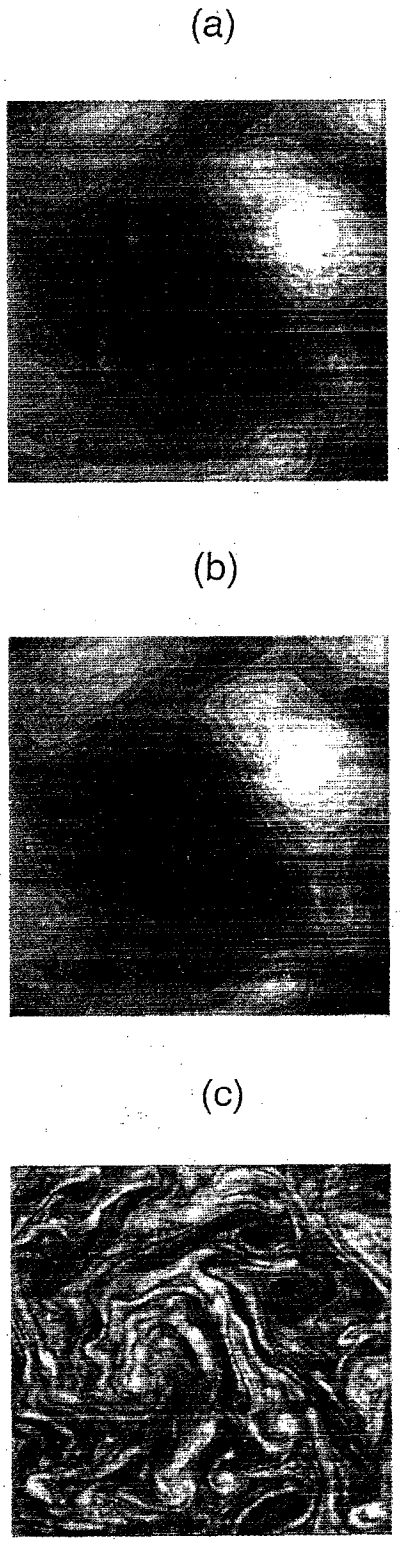

FIG. 3. Contour plots of the (a) potential $\tilde{\phi}(x,y)$, (b) density $\tilde{n}(x,y)$, and (c) vorticity fluctuations $\tilde{\Omega}(x,y)$ at the same instant of time in a saturated turbulent state for $\mathscr{C}=5$, $\nu=10^{-8}$, $K_0=0.15$, and 512^2 grid points. The figures show only the region $[0:\pi L]\times[0:\pi L]$.

FIG. 4. Contour plots of the (a) potential $\tilde{\phi}(x,y)$, (b) density $\tilde{n}(x,y)$, and (c) vorticity fluctuations $\tilde{\Omega}(x,y)$ at the same instant of time in a saturated turbulent state for $\mathscr{C}=0.1$, $\nu=10^{-8}$, $K_0=0.15$, and 512^2 grid points. The figures show only the region $[0:\pi L]\times[0:\pi L]$.

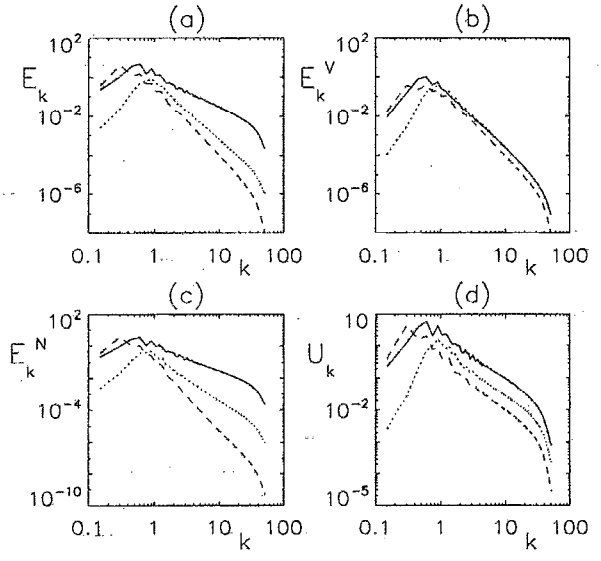

FIG. 5. (a) Total energy spectra E_k for $\mathscr{C}=0.1$ (full line), $\mathscr{C}=1$ (dots), and $\mathscr{C}=5$ (dashes). (b) Kinetic energy spectra E_k^V for $\mathscr{C}=0.1$ (full line), $\mathscr{C}=1$ (dots), and $\mathscr{C}=5$ (dashes). (c) Density energy spectra E_k^N for $\mathscr{C}=0.1$ (full line), $\mathscr{C}=1$ (dots), and $\mathscr{C}=5$ (dashes). (d) Enstrophy spectra U_k for $\mathscr{C}=0.1$ (full line), $\mathscr{C}=1$ (dots), and $\mathscr{C}=5$ (dashes).

cade model predicts[16] a spectral exponent of 3, and it is to be noted that in a high-k inertial range, the Hasegawa–Mima enstrophy, $|(1+k^2)\tilde{\phi}_{\mathbf{k}}|^2$, is indistinguishable from the 2-D Navier–Stokes mean-squared vorticity, $|k^2\tilde{\phi}_{\mathbf{k}}|^2$. This k^{-3} spectral energy power law has been observed for large-scale motion in the atmosphere,[17] a well-defined case of driven turbulence, which is nearly two dimensional, and it has been suggested by simulations of the Hasegawa–Mima and Hasegawa–Wakatani systems that were less well resolved.[6,5,18]

Numerical simulations of 2-D Navier–Stokes turbulence, in general, exhibit a steeper energy spectrum, for instance, $\alpha_V\simeq 4.3$ in decaying turbulence,[19,20] or $\alpha_V\simeq 3.5-4.5$ in stationary turbulence, depending on the stirring (low-k external driving). The origin of this discrepancy can be traced to the presence of pronounced coherent structures. If the turbulence is driven with a random forcing, which inhibits the formation of such structures, the energy spectrum is found to be consistent with the self-similar cascade model,[21] agreeing with the present work and the driven cases cited above. In decaying turbulence, $\alpha_V\simeq 3$ is actually observed in an early phase, before the appearance of pronounced coherent vortex structures.[22] In the present case of gradient-driven, collisional drift-wave turbulence, the excitation represented by Γ_n is extended over a broad range in k, and is evidently sufficiently incoherent to prevent the formation of coherent structures, so that α_V remains close to the self-similar model in this case as well.

TABLE II. Decay exponents for the energy spectra.

$\mathscr{C}$	E_k	E_k^V	E_k^N	U_k
0.1	$k^{-1.6}$	$k^{-3.1}$	$k^{-1.6}$	$k^{-1.3}$
1.0	$k^{-2.9}$	$k^{-3.2}$	$k^{-2.7}$	$k^{-1.5}$
5.0	$k^{-3.5}$	$k^{-3.5}$	$k^{-4.2}$	$k^{-1.6}$

The form of the density spectrum, E_k^N, on the other hand, depends quite strongly on $\mathscr{C}$. In the hydrodynamic regime, $\mathscr{C} \ll 1$, the density behaves essentially as a passive scalar, in which case the self-similar cascade model, given the vorticity cascade model for the **E×B** eddies, suggests the form $E_k^N \sim k^2 E_k^V$, which is, in fact, observed: for $\mathscr{C}=0.1$, $E_k^V \sim k^{-3.5}$ and $E_k^N \sim k^{-1.6}$. The consequence is that in the hydrodynamic regime, the density spectrum E_k^N dominates the energy spectrum at high k. By contrast, in the adiabatic limit, $\mathscr{C} \gg 1$, the kinetic energy is dominant at high k, since $\tilde{n}$ is forced by the strong cross-coupling to have the same spectrum as $\tilde{\phi}$ (recall that $\tilde{\phi}$ is the **E×B** streamfunction).

It is therefore clear why the sensitivity of E_k to $\mathscr{C}$ is entirely due to that of E_k^N. This is completely consistent with the other results: in the hydrodynamic regime, $\tilde{n}$ decouples from $\tilde{\phi}$, and its component of the energy is efficiently transferred to small scales, broadening the spectrum, while in the adiabatic regime this part of the dynamics is suppressed by the cross-coupling of $\tilde{n}$ to $\tilde{\phi}$.

The angle-integrated enstrophy spectrum is defined as

$$U=\int dk\ U_k, \quad U_k=\sum_{\mathbf{k}} \frac{1}{2}|\tilde{n}_{\mathbf{k}}+k^2\tilde{\phi}_{\mathbf{k}}|^2,$$

$$|\mathbf{k}| \in [k-\Delta k, k+\Delta k]. \tag{36}$$

Like the energy spectrum, U_k has a maximum at k_0 and follows a power law for $k>k_0$. For U_k, the variation of the spectral indices with $\mathscr{C}$ is much smaller than that for E_k. The reason is that U_k is dominated by the component, due solely to the vorticity, as this involves a much high power of k, and we have already established the insensitivity of E_k^V to $\mathscr{C}$. Up to a correction due to E_k^N that is negligible, especially in the hydrodynamic regime, the spectral indices of U_k are given approximately by those of the vorticity.

For the total energy, E, two other spectral distributions were studied:

$$E=\int dk_x\ E(k_x)=\int dk_y\ E(k_y). \tag{37}$$

The energy spectra of $E(k_x)$ and $E(k_y)$, for $\mathscr{C}=5$ is shown in Fig. 6. For $k_x, k_y > k_0$, the spectral distribution is isotropic, while for $k_x, k_y \lesssim k_0$, it is anisotropic. The contour plots of γ as a function of $\mathbf{k}$ have a similar form as those of $E_{\mathbf{k}}$ for $k<k_0$, showing that the behavior for $k<k_0$ is essentially determined by linear forcing, since γ is proportional to k_y and maximum at $\mathbf{k}_m=(0,k_m)$. For $\mathscr{C} \ll 1$, we find that $k_0=k_m$, while for $\mathscr{C}>1$, where k_m becomes constant at about 1.3, the actual spectrum peak drops to lower k as $\mathscr{C}$ increases. This is another clear result of the inverse energy cascade in the adiabatic regime.

VI. COMPARISON TO QUASILINEAR THEORY

An interesting aspect of any turbulence study is to determine the importance of the nonlinear terms in establishing the turbulent state. A standard way of analyzing how well the linear properties characterize the system is to compare nonlinear quantities with corresponding quasilinear and linear quantities. Such a comparison is usually done only with the

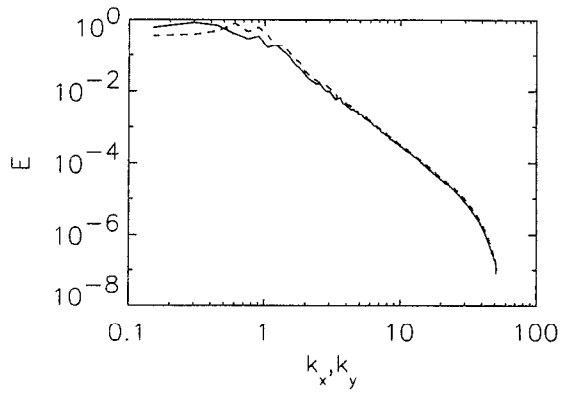

FIG. 6. Energy spectra for $\mathscr{C}=5$ $E(k_x)$ (full line) and $E(k_y)$ (dashes).

turbulent density flux, often in order to decide from a given level of turbulence in an experiment whether the inferred quasilinear flux can account for the actual one. This methodology is often carried over into theoretical studies as well.[8] In the present work, however, we also measure the actual phase shift and relative amplitude of the density fluctuations to those in the potential, in order to discern explicitly whether the often-employed linear response model is valuable.

Regarding the flux, although the quantity Γ_n defined in Eq. (11) is properly the rate at which the fluctuations obtain free energy from the density gradient, it is also equal to the turbulent density flux, since ∇n is unity in normalized units. We therefore refer to Γ_n as the turbulent flux in this section.

The angle-integrated turbulent flux spectrum is defined as in Eq. (34), in terms of

$$\Gamma_{n\mathbf{k}}=ik_y\tilde{n}_{\mathbf{k}}\tilde{\phi}_{\mathbf{k}}^*, \tag{38}$$

and for its quasilinear analog, here for convenience called the quasilinear flux,

$$\Gamma_{\mathbf{k}}^{\mathrm{ql}}=ik_y(1+f_{\mathbf{k}})|\tilde{\phi}_{\mathbf{k}}|^2, \tag{39}$$

where $f_{\mathbf{k}}$ is the linear response function defined in Eq. (27). In the adiabatic limit ($\mathscr{C} \gg 1$), $\Gamma_n \simeq \Gamma^{\mathrm{ql}}$, while for $\mathscr{C} \lesssim 1$, $\Gamma_n < \Gamma^{\mathrm{ql}}$ (see Table I). Their ratio, $\Gamma_n/\Gamma^{\mathrm{ql}}$, decreases with decreasing $\mathscr{C}$ approximately as $\Gamma_n/\Gamma^{\mathrm{ql}} \sim \mathscr{C}^{1/3}$ for $\mathscr{C} \lesssim 1$. Comparison of the spectral behavior of the two expressions shows that for $k \lesssim k_0$, $\Gamma_n(k) \simeq \Gamma^{\mathrm{ql}}(k)$ for all values of $\mathscr{C}$ (see Fig. 7).

This confirms the importance of the linear properties at long wavelength, for $k \lesssim k_0$, which was already observed in the energy spectrum. However, near the energy peak at $k \gtrsim k_0$, $\Gamma^{\mathrm{ql}}(k)$ exceeds $\Gamma_n(k)$ by a factor that increases with decreasing $\mathscr{C}$. In the adiabatic limit $\mathscr{C}=5$, both fluxes coincide over the entire spectrum. The agreement would seem somewhat surprising, since in this regime the (nonlinear) inverse cascade is still robust, and is particularly robust compared to the linear terms as these are weakened by the strong cross-coupling, which gives rise to an energy peak far to the low-k side of the most unstable mode ($k_0 \ll k_m$). On the other hand, this argument applies to the kinetic energy spectrum, since it is $\tilde{\phi}$, which is still turbulent, and hence to the total energy, since although E^N resides in $\tilde{n}$, it is put where it is in the spectrum by the inverse cascade for $\tilde{\phi}$. The response of $\tilde{n}$

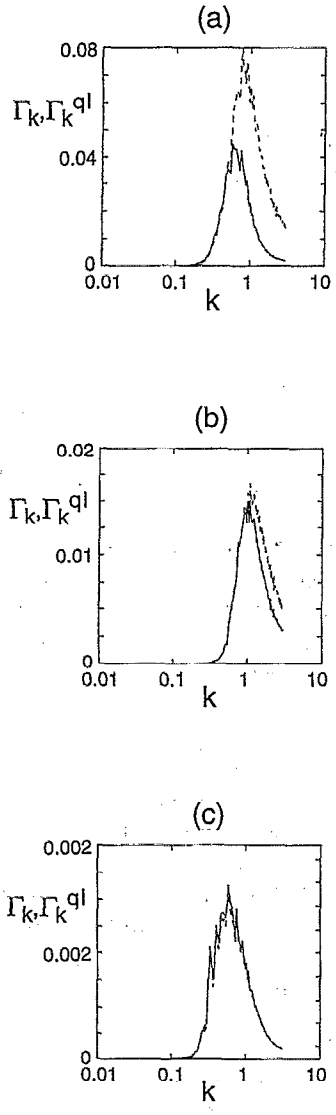

FIG. 7. Spectral behavior of the turbulent flux $\Gamma_n(k)$ (full line) and the quasilinear flux $\Gamma^{ql}(k)$ (dashed line) for (a) $\mathscr{C}=0.1$, (b) $\mathscr{C}=1$, and (c) $\mathscr{C}=5$, for 256^2 grid points, $K_0=0.0375$ and $\nu=10^{-4}$.

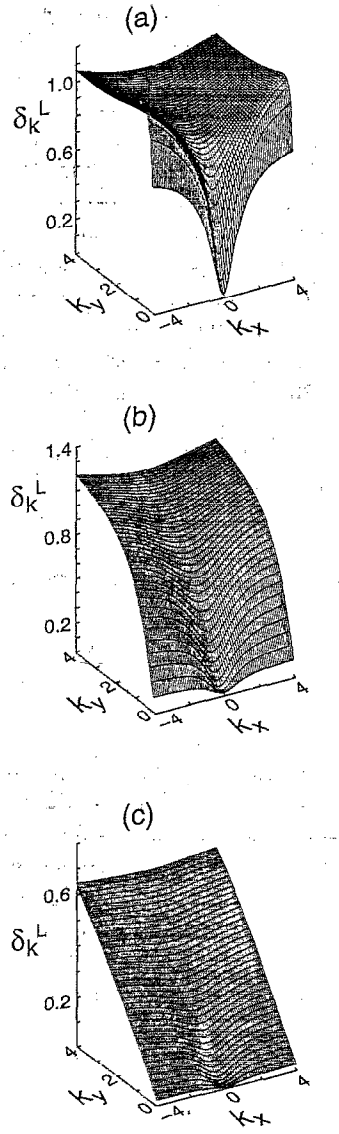

FIG. 8. Linear phase shifts δ_k^L, for (a) $\mathscr{C}=0.1$, (b) $\mathscr{C}=1$, and (c) $\mathscr{C}=5$, for 128^2 nodes and $K_0=0.15$.

to $\tilde{\phi}$ in the adiabatic regime is dominated by the cross-coupling, and so even though the fluctuations are turbulent, this part of their dynamics behaves essentially as it does for linear waves, which serves to explain the good agreement of $\Gamma_n(k)$ and $\Gamma^{ql}(k)$. One should not forget, however, that in evaluating Γ^{ql} we are taking the spectrum of $\tilde{\phi}$ as a given. That is, the apparent success of Γ^{ql} does not mean that linear physics determines Γ_n. What the good agreement between Γ_n and Γ^{ql} at low k shows is that although $\tilde{\phi}$ is nonlinear, the response of $\tilde{n}$ to it is linear, in the sense that the nonlinearity in Eq. (2) is weak compared to the forcing terms.

The linear and nonlinear phase shifts, δ_k^L and δ_k, were defined in Eqs. (30) and (29). The k dependence of these quantities for $\mathscr{C}=0.1$, 1, 5, and 128^2 nodes are shown in Figs. 8 and 9, respectively. In all cases the nonlinear phase shifts are time averaged over the saturated state.

For linear waves, the two quantities that oppose the tendency of the parallel dissipation ($\mathscr{C}$) to enforce adiabaticity are the density gradient (∇n) and the ion inertia ($k_\perp \rho_s$). These are weakest at the lowest k [mode (1,1)], so one sees the weakest phase shifts there. For large $\mathscr{C}$, the k_x dependence disappears, because the inertia with its higher k dependence is the dominant phase-shift producing effect.

For the turbulence, $\mathbf{E}\times\mathbf{B}$ advection is also present to oppose the parallel dissipation, and this is obviously more important in the hydrodynamic regime. What is interesting is that this produces low phase shifts, and the reason it does so is that the turbulent advection tends to randomize the relationship of $\tilde{n}$ to $\tilde{\phi}$. When the $\mathbf{E}\times\mathbf{B}$ advection is dominant, as at high k and low $\mathscr{C}$, the two fluctuations become statistically independent. For low $\mathscr{C}$ the phase shift is strongest at low k, because ∇n is relatively strongest there, and because the opposite cascade tendencies of $\tilde{\phi}$ and $\tilde{n}$ ensure that $\tilde{\phi}$ is significantly larger than $\tilde{n}$ there. It drops toward zero else-

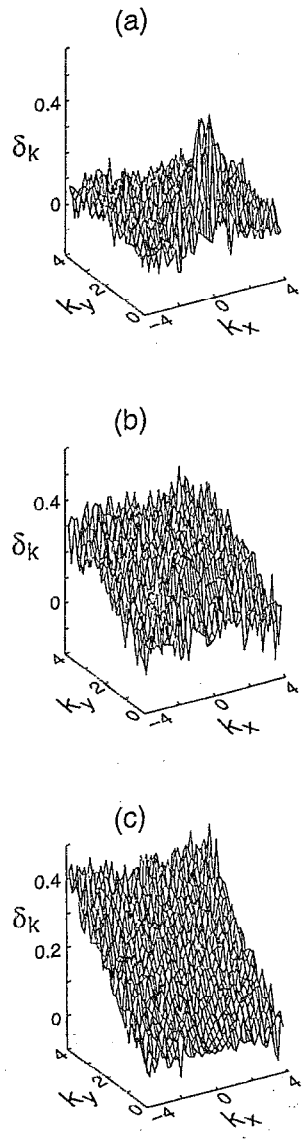

FIG. 9. Nonlinear phase-shifts $\delta_{\mathbf{k}}$, for (a) $\mathscr{C}=0.1$, (b) $\mathscr{C}=1$, and (c) $\mathscr{C}=5$ for 128^2 nodes and $K_0=0.15$.

where because the $\mathbf{E}\times\mathbf{B}$ advection everywhere dominates both the parallel dissipation and ∇n (in contrast to the resulting k dependence against the linear case). As $\mathscr{C}$ rises, the randomizing tendency of the advection is progressively weaker, and the stronger inertia at high k causes a larger phase shift.

Because of the importance of the dependence of the amplitude ratio $\tilde{n}/\tilde{\phi}$ on $\mathscr{C}$ and k, it should be clear then that $\delta_{\mathbf{k}}$ is not a good way of evaluating the adiabaticity, as is usually done, and the concepts of adiabaticity and phase difference should be clearly distinguished.

In analogy to the linear response function $f_{\mathbf{k}}$ given by Eqs. (27) and (26), it is possible to define a nonlinear response function $\mathscr{F}_{\mathbf{k}}$ as

$$\tilde{n}_{\mathbf{k}}=(1+\mathscr{F}_{\mathbf{k}})\tilde{\phi}_{\mathbf{k}}, \tag{40}$$

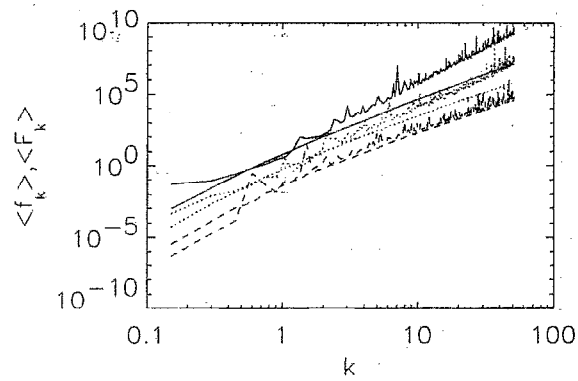

FIG. 10. Comparison of the average nonlinear response $\langle\mathscr{F}_{\mathbf{k}}\rangle$ and the average linear response $\langle f_{\mathbf{k}}\rangle$ for $\mathscr{C}=0.1$ (full line), $\mathscr{C}=1$ (dots), and $\mathscr{C}=5$ (dashes).

$$\mathscr{F}_{\mathbf{k}}=\frac{\tilde{n}_{\mathbf{k}}\tilde{\phi}_{\mathbf{k}}^{*}}{|\tilde{\phi}_{\mathbf{k}}|^{2}}-1, \tag{41}$$

which gives a measurement of how much $\tilde{n}_{\mathbf{k}}$ and $\tilde{\phi}_{\mathbf{k}}$ differ. As expected, $\mathscr{F}_{\mathbf{k}}$ and $f_{\mathbf{k}}$ are larger in the hydrodynamic regime ($\mathscr{C}=0.1$), decreasing as $\mathscr{C}$ increases and for a fixed value of $\mathscr{C}$, they increase toward high-k values. For high k, $\mathscr{F}_{\mathbf{k}}\sim k^{\epsilon}$, where ϵ varies from 3.4 (for $\mathscr{C}=5$) to 4.7 (for $\mathscr{C}=0.1$). In Fig. 10, the average nonlinear and the linear response functions are compared for $\mathscr{C}=0.1$, 1, and 5, with the best agreement for $\mathscr{C}=5$, as also occurred for the turbulent and quasilinear fluxes. It is interesting to note that the imaginary parts of the nonlinear and linear response functions have a better agreement than the real parts. When calculating $\Gamma_n(k)$ and $\Gamma^{\mathrm{ql}}(k)$, only the imaginary parts of $\mathscr{F}_{\mathbf{k}}$ and $f_{\mathbf{k}}$ are used, this helps explaining the good agreement between the turbulent and quasilinear fluxes.

VII. STATISTICAL PROPERTIES

By statistical properties, we refer to measures of the statistical independence of different components of the system. These measures can be used to examine the usefulness of analytical models of turbulence that rely on a sufficient degree of randomness to validate expansions about a Gaussian distribution of, e.g., relative phases. For example, simple analysis of the dissipation-free analog of Eqs. (1) and (2) using a cascade model was successful in explaining the spectrum of Γ_n.[7] In that case, the phase-shift distribution is nearly random and uniform, with a small shift toward positive values caused by the density gradient acting on the turbulence in the inertial range, and the amplitude distribution is Gaussian. But in a different system, collisional drift wave turbulence in a sheared magnetic field, departures from a Gaussian amplitude distribution reflected important components of the system's dynamics.[11] It is therefore clearly important to develop quantitative measures of the statistical properties in order to make clear judgments concerning the usefulness of specific analytical models.

One such measure is that of the normalized structure functions of spatial increments of the physical quantities of

interest.[23] In the present case, we measure these functions for the density, potential, and vorticity, increments $\delta\tilde{n}_r$, $\delta\tilde{\phi}_r$, and $\delta\tilde{\Omega}_r$, defined as

$$\delta\tilde{n}_r=\tilde{n}(\mathbf{x}+\mathbf{r})-\tilde{n}(\mathbf{x}), \tag{42}$$

$$\delta\tilde{\phi}_r=\tilde{\phi}(\mathbf{x}+\mathbf{r})-\tilde{\phi}(\mathbf{x}), \tag{43}$$

$$\delta\tilde{\Omega}_r=\tilde{\Omega}(\mathbf{x}+\mathbf{r})-\tilde{\Omega}(\mathbf{x}), \tag{44}$$

where

$$\mathbf{r}=r\hat{\mathbf{x}}, \quad \text{or,} \quad \mathbf{r}=r\hat{\mathbf{y}}. \tag{45}$$

The normalized structure functions for these increments are defined as

$$F^{(2j)}=\frac{\langle(\delta\tilde{n}_r)^{2j}\rangle}{\langle(\delta\tilde{n}_r)^2\rangle^j}, \tag{46}$$

$$G^{(2j)}=\frac{\langle(\delta\tilde{\phi}_r)^{2j}\rangle}{\langle(\delta\tilde{\phi}_r)^2\rangle^j}, \tag{47}$$

$$H^{(2j)}=\frac{\langle(\delta\tilde{\Omega}_r)^{2j}\rangle}{\langle(\delta\tilde{\Omega}_r)^2\rangle^j}, \tag{48}$$

where the angled brackets indicate ensemble averages. In our calculations, we consider $r=2^m 2\pi L/N$, where $N^2=2^{2j}$ is the number of grid nodes and $L=2\pi/K_0$, such that $r_{\min}=4\pi L/N$ (for $m=1$) and $r_{\max}=\pi L$, (for $m=j-1$), with r is given in units of ρ_s. In order to study the small-scale statistical properties, we considered a relatively small box size, $K_0=0.15$, and high-spatial resolution, 1024^2 nodes, such that $r_{\min}\simeq 0.08$ and $r_{\max}\simeq 21$. Since the turbulence is isotropic (cf. Fig. 6), we calculate the structure functions in both x and y directions and average in order to improve statistics. In Fig. 11, we show the structure functions of density, potential, and vorticity, and compare them to the corresponding Gaussian values. While the large-scale statistics (for $r\gtrsim k_0^{-1}$) are essentially Gaussian (in fact, as discussed below, almost perfectly Gaussian), statistics become increasingly non-Gaussian for $r<k_0^{-1}$. This indicates the existence of small-scale intermittency: "intermittency" refers to the fact that fluctuations of a particular scale, r, fill less space than those of scale $2r$, and so on. This feature of the turbulence is reflected by the fact that the structure functions are larger, both for smaller scale r and for higher-order j: at the smallest scales the contributions to the moment integrals are dominated by the largest values, arising from a small fraction of the total area.

While F^{2j} and H^{2j} show a clear power-law behavior with $F^{2j}\sim r^{\beta_j}$ and $H^{2j}\sim r^{\kappa_j}$, the structure functions of the potential H^{2j} are approximately Gaussian, even for the smallest scales and practically independent of $\mathscr{C}$. The structure of the density, on the other hand, depends strongly on $\mathscr{C}$, as we have already learned from the contour plots and spectra. In the hydrodynamic regime we find $\beta_j\sim\kappa_j$, but for the transition case ($\mathscr{C}=1$) there appears a slight departure, $\beta_j\sim 1.5\kappa_j$. In the adiabatic regime the departure widens: $\beta_j\sim 0$, while κ_j is, like other properties measured concerning $\tilde{\phi}$, independent of $\mathscr{C}$. We do find, however, that both β_j and κ_j increase with j more strongly than linearly, which indicates a multifractal behavior, as is well known for hydrodynamic turbulence (see, e.g., Ref. 24).

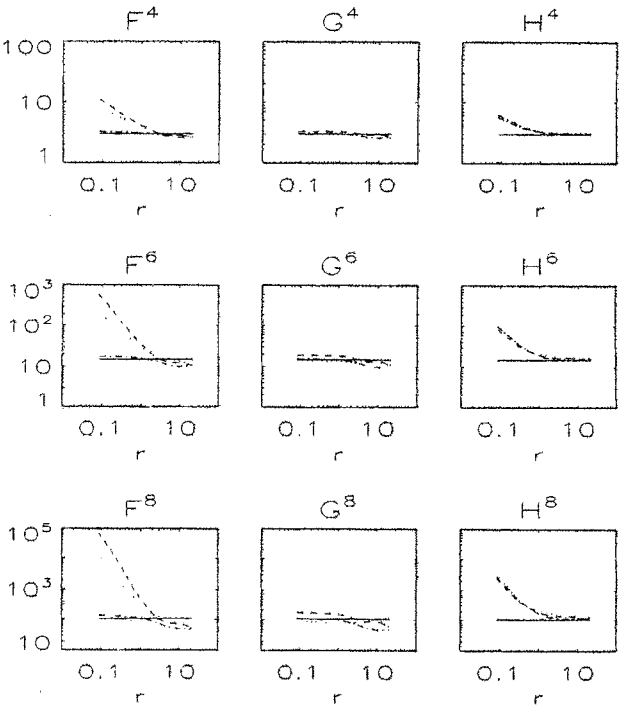

FIG. 11. Density (F^{2j}), potential (G^{2j}), and vorticity (H^{2j}) structure functions for $j=2$, 3, 4, $K_0=0.15$, and $\mathscr{C}=0.1$ (dots), $\mathscr{C}=1$ (dashes), $\mathscr{C}=5$ (dots/dashes), and Gaussian values (full line).

In the results just described, the ensemble averages of the large-scale component are not very accurate statistically, since the computations were not continued for sufficiently long times. In order to obtain better averages for large scales, numerical simulations with a larger box size ($K_0=0.0375$), and only 256^2 nodes were performed. These cases were carried for many large-eddy turnover times τ_0, where $\tau_0\equiv(uk_0)^{-1}$ and $u^2\equiv E^V/2\pi$. For the adiabatic case $\mathscr{C}=5$, which is the one with the slowest response time of the three as discussed earlier, $\tau_0\simeq 10$, and the computations were carried for $t\simeq 50\tau_0$ following an already-established saturated state. In this case, $r_{\min}\simeq 1.3$ and $r_{\max}\simeq 84$. Only the results for $\mathbf{r}=r\hat{\mathbf{x}}$ are shown, since for $\mathbf{r}=r\hat{\mathbf{y}}$ they were virtually identical, in spite of the anisotropy of the spectrum for $r\lesssim k_0^{-1}$. The large-scale structure functions are shown in Fig. 12, where it can be seen that they are almost perfectly Gaussian. This behavior is consistent with the absence of large-scale coherent structures. On the other hand, similar diagnostics performed on cases reproducing the calculations of Ref. 8, which considered much more strongly viscous conditions, long-living coherent structures were observed, and the statistics were far from Gaussian. For the weakly dissipative conditions considered here, these structures disappear, most likely a consequence of the presence of an extended inertial range and the high level of small-scale turbulence which that entails.

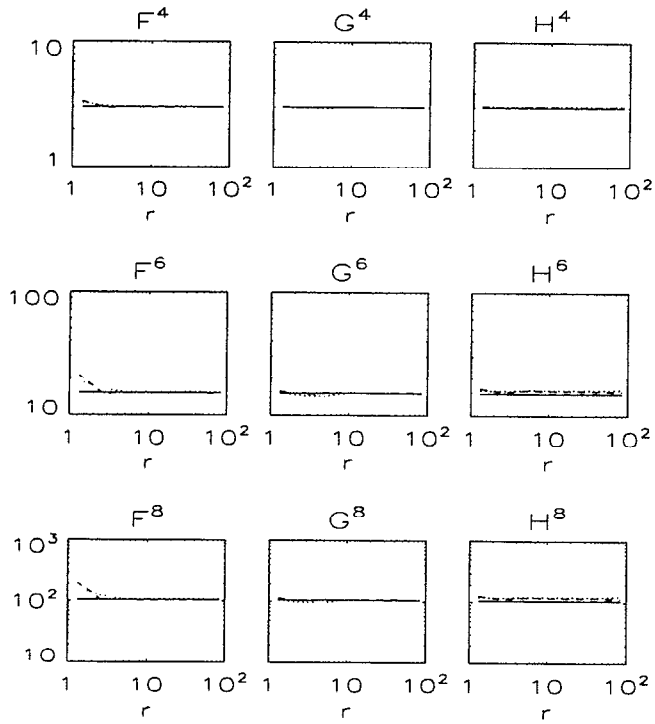

FIG. 12. Density (F^{2j}), potential (G^{2j}), and vorticity (H^{2j}) structure functions for $j=2, 3, 4$, $K_0=0.0375$, $\mathbf{r}=r\hat{\mathbf{x}}$, and $\mathscr{C}=0.1$ (dots), $\mathscr{C}=1$ (dashes), and Gaussian values (full line).

VIII. SPECTRAL TRANSFER OF FLUCTUATION ENERGY

Discussion of the results up to this point has revealed much of the basic character of the turbulence resulting from the Hasegawa–Wakatani system. Increased intermittency and departure from simple quasilinear theory at small scales for $\mathscr{C}\lesssim 1$ reflects the importance of the density nonlinearity $(\mathbf{v}_E\cdot\nabla\tilde{n})$, as the cross-coupling between $\tilde{n}$ and $\tilde{\phi}$ is weakened. Indeed, $\mathbf{v}_E\cdot\nabla\tilde{n}$ vanishes as $\mathscr{C}$ becomes arbitrarily large. One can argue as previously[9] that the tendency of turbulent advection of $\tilde{n}$, which, except for the cross-coupling would behave as a passive scalar, is to cascade toward small scales. Theory and simulation of statistical equilibrium ensembles show this clearly in the limited case of truncated, dissipation-free systems.[7] However, one would like a quantitative demonstration that this physics carries over into more realistic systems such as that under study here.

A useful diagnostic for this purpose is to directly measure the spectral transfer function for the fluctuation energy, E, defined in Eq. (7). This was done for three-dimensional, incompressible, neutral-fluid turbulence by Domaradzski,[25] giving quantitative demonstration that the basic equations of fluid turbulence actually displayed the local, direct energy cascade long known from the Kolmogorov eddy-mitosis model and laboratory experiments[26] (this is, of course, in contrast to the two-dimensional cases cited in Sec. V). That is, energy transferred into a given spectral range, between $k-dk$ and $k+dk$, was seen in the simulations to have originated from wave numbers k' for which $k\sim 2k'$. Note that in the neutral-fluid case, E is indeed the fluid kinetic energy.

For the present purpose, the transfer function is computed separately for each nonlinearity, viz.,

$$\frac{\partial E^V(\mathbf{k})}{\partial t}=\sum_{\mathbf{k}'} T^V(\mathbf{k}\leftarrow\mathbf{k}')+\text{linear terms}, \tag{49}$$

$$\frac{\partial E^N(\mathbf{k})}{\partial t}=\sum_{\mathbf{k}'} T^N(\mathbf{k}\leftarrow\mathbf{k}')+\text{linear terms}, \tag{50}$$

$$\frac{\partial W(\mathbf{k})}{\partial t}=\sum_{\mathbf{k}'} T^W(\mathbf{k}\leftarrow\mathbf{k}')+\text{linear terms}, \tag{51}$$

where the spectral transfer of fluid kinetic energy from mode $\mathbf{k}'$ to mode $\mathbf{k}$ is

$$T^V(\mathbf{k}\leftarrow\mathbf{k}')=2\ \mathrm{Re}(k_xk_y'-k_x'k_y)\tilde{\phi}_{-\mathbf{k}}\tilde{\Omega}_{\mathbf{k}-\mathbf{k}'}\tilde{\phi}_{\mathbf{k}'},$$

and that of density fluctuation activity from mode $\mathbf{k}'$ to mode $\mathbf{k}$ is

$$T^N(\mathbf{k}\leftarrow\mathbf{k}')=2\ \mathrm{Re}(k_xk_y'-k_x'k_y)\tilde{n}_{-\mathbf{k}}\tilde{\phi}_{\mathbf{k}-\mathbf{k}'}\tilde{n}_{\mathbf{k}'},$$

while the transfer of mean-squared vorticity from mode $\mathbf{k}'$ to mode $\mathbf{k}$ is

$$T^W(\mathbf{k}\leftarrow\mathbf{k}')=2\ \mathrm{Re}(k_xk_y'-k_x'k_y)\tilde{\Omega}_{-\mathbf{k}}\tilde{\phi}_{\mathbf{k}-\mathbf{k}'}\tilde{\Omega}_{\mathbf{k}'}.$$

In each case, mode $\mathbf{k}$ refers to a specific Fourier component pair (k_x,k_y), and due to the condition that $\tilde{\phi}$ and $\tilde{n}$ be real functions of position, mode $-\mathbf{k}$ is given by the complex conjugate of mode $\mathbf{k}$, and so the expressions involve both beat modes, $\mathbf{k}+\mathbf{k}'$ and $\mathbf{k}-\mathbf{k}'$. The transfer functions for each nonlinearity are defined separately because one is interested not only in the evolution of the total energy, as in Ref. 9, but in the relative importance and individual properties of each of the nonlinear processes in the system as well as the evolution of each independent fluctuating quantity, as in Ref. 7 and herein.

Since in a homogeneous system, one is interested in scale transfer, the salient quantities are those that give the transfer between ranges of scales, or between "shells" of modes (corresponding to the angle integrations for the spectra). For example, the scale transfer of E^V is given as $T^V(k\leftarrow k')$, where, in each instance, k refers to a range $[k-\Delta k,k+\Delta k]$, with Δk a fixed interval. Here, Δk is set to $0.5K_0$, as usual.

After each of the three cases described in previous sections, $\mathscr{C}=0.1$, $\mathscr{C}=1$, and $\mathscr{C}=5$, reached saturation, the energy transfer functions were computed. Due to the incoherent nature of the turbulence, time averages over a range $\Delta t=100$ were taken in order to provide good statistics. The results are shown in Figs. 13–15 and summarized in Table III. In the figures, contours of $T(k\leftarrow k')$ are shown only where it is positive, since antisymmetric about the line $k=k'$, corresponding to the exchange $(k\leftrightarrow k')$ is clear (this line is the dashed line drawn in the figures). Further clarifying the behavior of $T(k\leftarrow k')$ is the surface of T as a function of k and k'. In Table III, the maximum of each $T(k\leftarrow k')$ is given, normalized to the saturated total energy, E. Noteworthy in the figures is the local character of the spectral transfer: Most of the activity is close to the $k=k'$ line, which shows that the transfer occurs between scales of

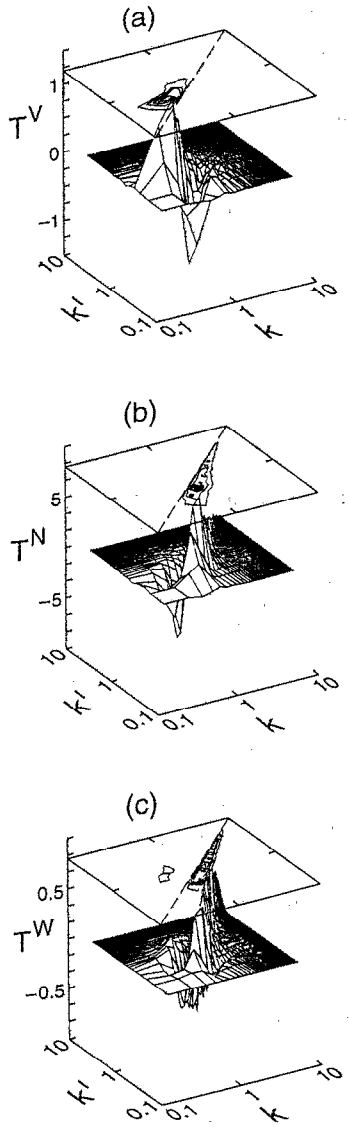

FIG. 13. Spectral transfers T^V, T^N, and T^W for $\mathscr{C}=0.1$, 128^2 nodes and $K_0=0.15$.

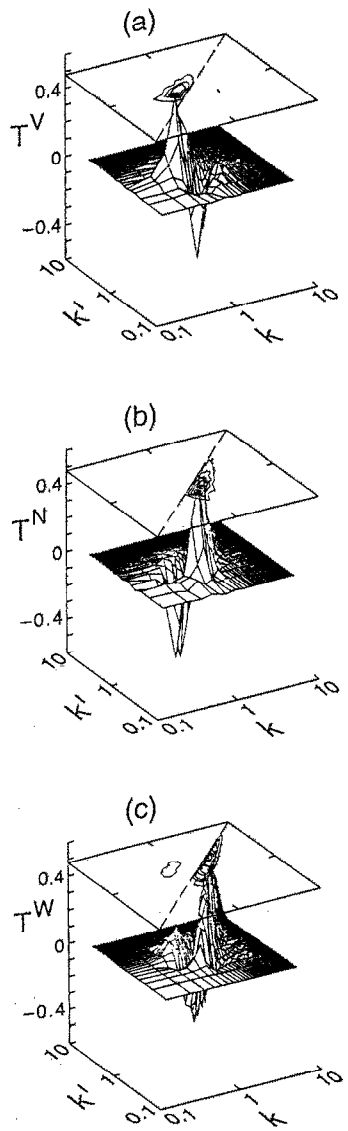

FIG. 14. Spectral transfers T^V, T^N, and T^W for $\mathscr{C}=1$, 128^2 nodes and $K_0=0.15$.

motion that are within a factor of 2 of each other; the transfer may be properly described as a local cascade. The positive contours in T^V lie above the $k=k'$ line, while in T^W they lie below it, showing that the **E×B** nonlinearity exhibits the familiar dual cascade of a 2-D fluid: toward large scales (inverse) for energy and toward small scales (direct) for vorticity. Similarly, T^N shows the direct cascade one expects since $\tilde{n}$ is passively advected by the **E×B** flow eddies.

Although the character of the system differs substantially between the adiabatic and hydrodynamic limits, the function and actual behavior of each nonlinearity remains the same throughout. Only the magnitude of T^N is sensitive to $\mathscr{C}$; this merely reflects that for high $\mathscr{C}$ the system is tightly constrained against strong departures from electron adiabaticity. This shows that it would be improper to speak of a change in the cascade tendency for total energy as $\mathscr{C}$ varies from small to large. Rather, it is correct to note the unchanged cascade tendencies of each nonlinearity, but that their relative magnitudes are affected by the strength of the cross-coupling. The results of investigating the energy transfer dynamics serve to solidly confirm the arguments to this effect made on the basis of absolute equilibrium ensembles in Ref. 7.

IX. CONCLUSION

In this paper, the detailed physical properties that determine the saturated turbulent state resulting from the Hasegawa–Wakatani resistive drift-wave model were studied. The system was solved using high-resolution numerical simulations in the nonviscous limit, such that the strength of the dissipative cross-coupling, $\mathscr{C}$, between the two fluctuating variables, $\tilde{n}$ and $\tilde{\phi}$, is the controlling parameter. The

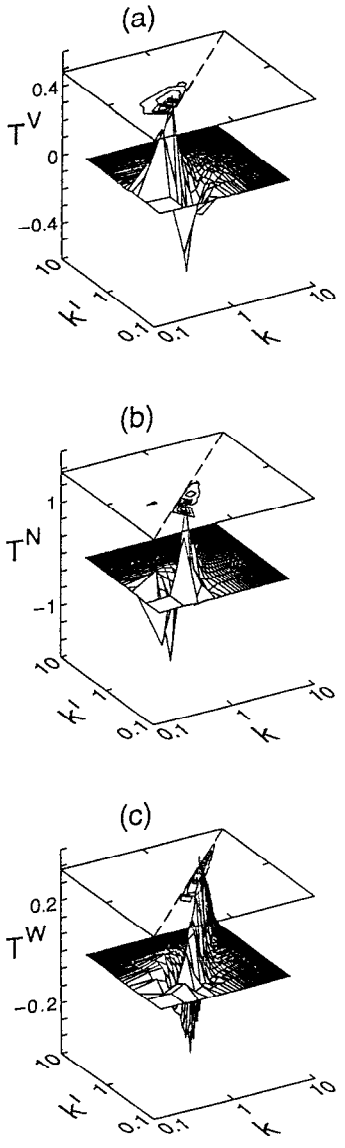

FIG. 15. Spectral transfers T^V, T^N, and T^W for $\mathscr{C}=5$, 128^2 nodes and $K_0=0.15$.

characteristics of the turbulence are quite different in the two regimes, hydrodynamic and adiabatic, corresponding to large and small $\mathscr{C}$, respectively. Nevertheless, the various diagnostics employed, especially the direct measurement of the energy transfer spectra, has shown that each of the essential ingredients of the system—gradient driving, dissipative cross-coupling, and turbulent **E×B** advection—all act with the same qualitative effect in all regimes, while the marked contrasts in the actual results reflect only that the relative strengths of these ingredients changes with the value of $\mathscr{C}$.

TABLE III. Maxima of the spectral transfer rates as functions of $\mathscr{C}$.

$\mathscr{C}$	T^V	T^N	T^W
0.1	1.10	7.04	0.71
1.0	0.46	0.54	0.47
5.0	0.51	1.55	0.39

Two overall features of the system stand out in importance. First, it becomes clear that nonlinear processes are of central importance to such quantitative measures as the saturated amplitudes and the transport produced by the turbulence. Not only would these not reflect scalings predicted by the results for linear waves, even the trends with $\mathscr{C}$ one would expect from linear analysis do not result: most prominently, the fact that the fluctuation energy level in saturation is lowest for the case with the intermediate linear growth rate. Even for the case in which the quasilinear flux estimate seems to be reasonable, the adiabatic regime with $\mathscr{C}=5$ where the growth rates and phase shifts are small, the turbulence is very strong and shifted to long wavelength by the robust dual energy/enstrophy cascade for $\tilde{\phi}$. The quasilinear procedure takes the fluctuation spectrum as given; it gives no method to calculate the spectrum, and simple linear mixing models fail to do so. Although to the long-wavelength side of the energy peak at $k=k_0$ the turbulence is anisotropic and highly influenced by the linear properties of the system, the nonlinear effects are still important. On the other hand, the cross-coupling that makes such a difference between regimes is of obvious importance. The result is such to make it highly unlikely that simplified expansion procedures that take one or another effect as "the dominant one" will be useful in capturing the essential dynamics of this system, or even in providing simple estimates of fluctuation levels and transport.

The other feature is the role played by the differing scales, which makes it important that computations of drift-wave turbulence be of high resolution (also see Ref. 11). The most obvious manifestation of this is the disappearance of coherent structures when the viscous damping is reduced. This allows the dissipative mechanisms to force the turbulence sufficiently that highly ordered structure does not form, which would mitigate against expectations of such structure forming in the more complicated setting of tokamak edge turbulence, which is even less viscous than the simulations presented here. Isolated, large coherent structures observed in more strongly viscous conditions (drift-wave turbulence) or in purely inertial ones (2-D Navier–Stokes turbulence) seem to have no role in this setting.

It is interesting to note that when the quasilinear flux estimate fails, it does so in the direction of overestimation. This is because the density tends to get randomized with respect to the potential in the strongly nonlinear, nonadiabatic regime. So, the average phase shift is less than a linear estimate would suggest, especially at the smaller scales, where turbulent advection overwhelms linear forcing. That the small-scale phase shift is larger when the electrons are adiabatic, also quite counterintuitive from the standpoint of linear theory, serves to underscore the importance of nonlinear effects in producing trends, as well as to the basic character.

The statistical structure of the large scales is almost perfectly Gaussian, which is in agreement with the absence of the isolated large coherent structures. The increasingly non-Gaussian density and the vorticity structure functions seen at

a smaller scale indicate the onset of intermittency as one enters the inertial range. This seems merely the effect of the cascade process of these quantities toward small-scale dissipation, and is not strongly reflected in the system energetics.

ACKNOWLEDGMENTS

One of the authors (S. J. C.) would like to thank Michael K. Tippett for the computational support.

[1]P. C. Liewer, Nucl. Fusion **25**, 543 (1985).
[2]W. Horton, Phys. Rep. **192**, 1 (1990).
[3]A. J. Wooton, B. A. Carreras, H. Matsumoto, K. McGuire, W. A. Peebles, Ch. P. Ritz, P. W. Terry, and S. J. Zweben, Phys. Fluids B **2**, 2879 (1990).
[4]A. Hasegawa and M. Wakatani, Phys. Rev. Lett. **50**, 682 (1985).
[5]M. Wakatani and A. Hasegawa, Phys. Fluids **27**, 611 (1984).
[6]A. Hasegawa and K. Mima, Phys. Fluids **21**, 87 (1978).
[7]B. D. Scott, H. Biglari, P. W. Terry, and P. H. Diamond, Phys. Fluids B **3**, 51 (1991).
[8]A. E. Koniges, J. A. Crotinger, and P. H. Diamond, Phys. Fluids B **4**, 2785 (1992).
[9]F. Y. Gang, B. D. Scott, and P. H. Diamond, Phys. Fluids B **1**, 1331 (1989).
[10]D. Biskamp, S. J. Camargo, and B. D. Scott, Phys. Lett. A **186**, 239 (1994).
[11]B. D. Scott, Phys. Fluids B **4**, 2468 (1992).
[12]S. I. Braginskii, in *Reviews of Plasma Physics*, edited by M. A. Leontovich (Consultants Bureau, New York, 1965), Vol. 1, p. 205.
[13]P. W. Terry and C. W. Horton, Phys. Fluids **26**, 106 (1983); R. E. Waltz, *ibid.* **26**, 169 (1983).
[14]B. D. Scott, Plasma Phys. Controlled Fusion **34**, 1977 (1992).
[15]B. D. Scott, J. Comput. Phys. **78**, 114 (1988).
[16]R. Fjörtoft, Tellus **5**, 225 (1953); R. H. Kraichnan, J. Fluid Mech. **47**, 525 (1971).
[17]P. R. Julian, W. M. Washington, L. Hembree, and C. Ridley, J. Atmos. Sci. **27**, 376 (1970).
[18]D. Fyfe and D. Montgomery, Phys. Fluids **22**, 246 (1979); A. Hasegawa, Y. Kodama, and C. Maclennan, *ibid.* **22**, 2122 (1979).
[19]R. Benzi, S. Patarnello, and P. Santangelo, J. Phys. A **21**, 1221 (1988).
[20]B. Legras, P. Santangelo, and R. Benzi, Europhys. Lett. **5**, 37 (1988).
[21]V. Borue, Phys. Rev. Lett. **71**, 3967 (1993).
[22]P. Santangelo, R. Benzi, and B. Legras, Phys. Fluids A **1**, 1027 (1989).
[23]C. W. Van Atten and W. Y. Chen, J. Fluid Mech. **44**, 145 (1970).
[24]G. Paladin and A. Vulpiani, J. Phys. A **21**, 1221 (1988).
[25]J. A. Domaradzski, Phys. Fluids **31**, 2747 (1988).
[26]L. T. Matveev, *Fundamentals of General Meteorology: Physics of the Atmosphere* (Israel Program for Scientific Translations, Jerusalem, 1967).